

## Biological evaluation, docking and molecular dynamic simulation of some novel diaryl urea derivatives bearing quinoxalindione moiety

Sedighe Sadeghian-Rizi<sup>1</sup>, Ghadam Ali Khodarahmi<sup>1</sup>, Amirhossein Sakhteman<sup>2</sup>,  
Ali Jahanian-Najafabadi<sup>3</sup>, Mahboubeh Rostami<sup>1</sup>, Mahmoud Mirzaei<sup>1,4</sup>,  
and Farshid Hassanzadeh<sup>1,\*</sup>

<sup>1</sup>Department of Medicinal Chemistry and Isfahan Pharmaceutical Sciences Research Center, School of Pharmacy and Pharmaceutical Sciences, Isfahan University of Medical Sciences, Isfahan, I.R. Iran.

<sup>2</sup>Department of Medicinal Chemistry, School of Pharmacy, Shiraz University of Medical Sciences, Shiraz, I.R. Iran.

<sup>3</sup>Department of Pharmaceutical Biotechnology, and Isfahan Pharmaceutical Sciences Research Center, School of Pharmacy and Pharmaceutical Sciences, Isfahan University of Medical Sciences, Isfahan, I.R. Iran.

<sup>4</sup>Bioinformatics Research Center, School of Pharmacy and Pharmaceutical Sciences, Isfahan University of Medical Sciences, Isfahan, I.R. Iran.

### Abstract

In this study a series of diarylurea derivatives containing quinoxalindione group were biologically evaluated for their cytotoxic activities using MTT assay against MCF-7 and HepG2 cell lines. Antibacterial activities of these compounds were also evaluated by Microplate Alamar Blue Assay (MABA) against three Gram-negative (*Escherichia coli*, *Pseudomonas aeruginosa* and *Salmonella typhi*), three Gram-positive (*Staphylococcus aureus*, *Bacillus subtilis* and *Listeria monocitogenes*) and one yeast-like fungus (*Candida albicans*) strain. Furthermore, molecular docking was carried out to study the binding pattern of the compounds to the active site of B-RAF kinase (PDB code: 1UWH). Molecular dynamics simulation was performed on the best ligand (16e) to investigate the ligand binding dynamics in the physiological environment. Cytotoxic evaluation revealed the most prominent cytotoxicity for 6 compounds with IC<sub>50</sub> values of 10-18 μM against two mentioned cell lines. None of the synthesized compounds showed significant antimicrobial activity. The obtained results of the molecular docking study showed that all compounds fitted in the binding site of enzyme with binding energy range of -11.22 to -12.69 kcal/mol vs sorafenib binding energy -11.74 kcal/mol as the lead compound. Molecular dynamic simulation indicated that the binding of ligand (16e) was stable in the active site of B-RAF during the simulation.

**Keywords:** Diaryl urea; Quinoxalindione; Docking; Cytotoxic; Molecular dynamic simulation; Sorafenib

### INTRODUCTION

Cancer is a major worldwide health problem and based on World Health Organization (WHO) report by 2030 more than 13 million cancer deaths will be expected (1,2). Chemotherapy is one of the most frequently used treatment for cancers but adverse side effects and resistance to the current chemotherapeutic agents are the major reasons for the failure in cancer chemotherapy (3). Thus, development of more efficient and less toxic anticancer agents remains an important issue in drug design (4). Diaryl urea derivatives have broad spectrum of biological effects and pharmaceutical functions. Several

diaryl urea derivatives such as sorafenib, regorafenib, linifanib and tivozanib have been so far synthesized and evaluated as the kinase inhibitors (Fig. 1). Sorafenib (BAY-43-9006), is the first orally bioavailable multiple kinase inhibitor approved by the U.S. Food and Drug Administration (FDA) and European Medicinal Agency (EMA) for the treatment of advanced renal cell carcinoma and hepatocellular carcinoma. It inhibits the kinase activity of both C-RAF and B-RAF (wild type and V600E mutant) with IC<sub>50</sub> values of 6.22 and 38 nM, respectively.

\*Corresponding author: F. Hassanzadeh  
Tel: +98-3137927096, Fax: +98-3116680011  
Email: hassanzadeh@pharm.mui.ac.ir

#### Access this article online



Website: <http://rps.mui.ac.ir>

DOI: 10.4103/1735-5362.217430

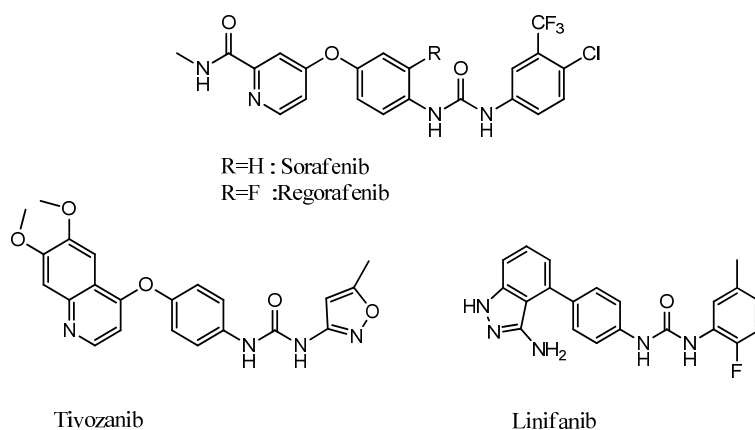


**Fig. 1.** Some examples of diaryl urea agents.

In addition, this molecule shows significant activity against several receptor tyrosine kinases (RTKs) involved in tumor cell proliferation and tumor angiogenesis including vascular endothelial growth factor receptor 2 and 3 (VEGFR-2 and VEGFR-3) and platelet-derived growth factor receptors (PDGFR- $\beta$ ) (5-7).

Introduction of a fluorine atom in the central phenyl ring of sorafenib led to the synthesis of regorafenib (BAY-73-4506), that has been approved by FDA for the treatment of colorectal cancer and gastrointestinal stromal tumor and inhibits C-RAF, V600E B-RAF and B-RAF with  $IC_{50}$  values of 2.5, 19 and 28 nM, respectively (8,9). Tivozanib (AV-951) hydrochloride is a potent and selective tyrosine kinase inhibitor of all three vascular endothelial growth factor receptors. It has been evaluated in several clinical trials including a phase II and phase III studies, demonstrating safety and efficacy for patients with advanced or metastatic renal cell carcinoma (10,11).

Linifanib (ABT-869) is a potent inhibitor of all VEGF and PDGF receptor tyrosine kinases that shows significant clinical activity as the monotherapy in patients with advanced hepatocellular carcinoma and inhibits kinase insert domain receptor (KDR) with an  $IC_{50}$  of 28 nM (12,13).

In this work, based on previous structure activity relationships (SARs) of sorafenib and its analogs we retained the diarylurea functionality as the key pharmacophore and focused our main modification on replacement

of pyridyl carboxamid group of sorafenib with quinoxalindione moiety in order to investigate the impact of increasing rigidity at the end of this backbone on the biological activities of the resulting compounds. Since antibacterial activities of quinoxalindione and diaryl urea derivatives have been reported separately, we were interested in investigating the antimicrobial activities of these new hybrid compounds with both pharmacophore moieties in a single scaffold (14-19).

In the present study 14 newly synthesized diaryl urea derivatives which were developed in our laboratory were evaluated for *in vitro* cytotoxicity and antimicrobial activities. The inhibitory activity of these compounds against two cancer cell lines including human breast cancer (MCF-7) and human liver cancer (HepG2) cell lines was evaluated using the standard 3-(4,5-dimethylthiazol-2-yl)-2,5-diphenyl tetrazolium bromide (MTT) assay. Antibacterial and anti-fungal activities of these compounds were screened by Microplate Alamar Blue Assay (MABA).

In order to investigate the interaction between B-Raf kinase inhibitors and B-Raf kinase, molecular dynamic simulation (MD) was performed on the best docking pose of the ligand with lowest binding energy. For this purpose, the protein structure was simulated in a grid box with water molecules and physiologic concentration of the salt. The binding pattern of the ligand after simulation was obtained. This fingerprint pattern can be helpful in the design of more potent molecules in future studies.

## MATERIALS AND METHODS

The following microorganisms were used as diluted samples with broth culture: *Staphylococcus aureus* PTCC 1337, *Bacillus subtilis* PTCC 1032, *Listeria. Monocytogenes* PTCC 1165, *Escherichia coli* PTCC 1338, *Pseudomonas aeruginosa* PTCC 1074, *Salmonella. Enteritidis* PTCC 1091 and *Candida albicans* PTCC 5027. All microorganisms were obtained from Persian Type Culture Collection (PTCC). Mueller-Hinton broth (Merk, Germany) and RPMI-1640 (Gibco, Scotland) were used for growth of bacteria and fungi, respectively. MTT, and dimethylsulfoxide (DMSO) were purchased from Merck, Germany.

Absorbances were determined with an ELISA plate reader (ELX 808, USA). MCF-7 cells were purchased from Pasteur Institute, Tehran, Iran. The stock solutions (10000  $\mu\text{M}$ ) of synthesized compounds were prepared by dissolving in DMSO and diluted with distilled water to achieve 10, 100, 250, 500  $\mu\text{M}$  concentrations. Since the primary stock was prepared in DMSO and then diluted to a ratio of at least 1/200, therefore, the highest concentration of DMSO in each cell would be less than 0.5% or even lesser.

### Biological activity procedures

#### *In vitro* cytotoxicity assay

MCF-7 and HepG2 cell lines were maintained respectively in RPMI-1640 and DMEM/F12 medium supplemented with fetal bovine serum (FBS) (10%, v/v) and antibiotics [penicillin (100 units/mL) and streptomycin (100 mg/mL)] in a humidified atmosphere of 5%  $\text{CO}_2$  at 37 °C (20,21). Briefly, after 2-3 subcultures, 180  $\mu\text{L}$  of the cells ( $4.5 \times 10^4$  and  $6 \times 10^4$  cells/mL of MCF-7 and HepG2, respectively) were seeded in triplicate on 96-well microplates and incubated for 24 h. Cells were treated with 20  $\mu\text{L}$  of different concentrations of the derivatives (10, 100, 250, 500  $\mu\text{M}$ ) for 48 h. The final concentrations of the compounds were 1, 10, 25, 50  $\mu\text{M}$  on the plate.

Sorafenib was used as the positive control and the wells containing cell suspension was regarded as the negative control. The blank

wells consisted of 200  $\mu\text{L}$  of the corresponding medium. The microplates were further incubated for 48 h. To evaluate cell survival, each well was then incubated with 20  $\mu\text{L}$  of MTT solution (5 mg/mL in PBS) for 3 h and the media in each well were replaced with 150  $\mu\text{L}$  DMSO. The absorbance of each well was measured at 570 nm using an ELISA reader. Each experiment was repeated three times. The percentage of cell viability was calculated using the following formula:

$$\text{Viable cells (\%)} = [(T-B)/(C-B)] \times 100$$

where, C is the absorbance of negative control, T is the absorbance of treated samples, and B is the absorbance of the blank. The  $\text{IC}_{50}$  values represent the mean of three independent experiments each performed in triplicate. Analysis of variance (ANOVA) followed by Tukey test was used to determine the differences between  $\text{IC}_{50}$  values of each compound and sorafenib as positive control. All results were expressed as mean  $\pm$  S.E.M and  $P < 0.05$  was considered as statistically significant.

#### Antibacterial and antifungal evaluation

The *in vitro* antibacterial and antifungal activities of the synthesized compounds were studied by MABA using 96-wells microplates (22,23).

At first, all tested microbial strains were sub-cultured overnight in a suitable medium (Mueller–Hinton agar for bacterial strains and Sabouraud dextrose agar for fungal pathogen) followed by their cultivation in the broth medium to obtain 0.5 McFarland standard turbidity ( $1.5 \times 10^8$  CFU/mL). Mueller-Hinton broth was used as medium for growth of bacteria.

Except negative control wells which should contain 160  $\mu\text{L}$  of medium, 140  $\mu\text{L}$  of culture medium poured into each well of 96-well plates.

Subsequently 20  $\mu\text{L}$  of each bacterial suspension was distributed in all 96 wells of microplate including positive control (containing microorganism and standard antibiotic) and negative control (containing microorganism and culture medium). Then 20  $\mu\text{L}$  of each concentration of the synthesized compounds were added to two neighbour wells

except for positive and growth control wells. After adding alamarBlue (20  $\mu$ L) to all of 96 wells the total volume in each well reaches to 200  $\mu$ L. The final concentrations of the tested compounds were 512, 256, 128, 64 and 32  $\mu$ g/mL. Plates were covered and sealed with para film and incubated for 24 h at 37  $^{\circ}$ C. After incubation, results were recorded as minimum concentration of each synthesized compound which completely inhibited growth of microorganism (MIC).

Antifungal activity was determined as antibacterial assay except with some modifications. The final size of inoculum was  $1.0 \times 10^6$  CFU/mL for fungi and the turbidity was measured spectrometrically at 580 nm. The antibacterial agent ciprofloxacin and antifungal agent fluconazole were used as the standard controls. All experiments were performed in triplicate and mean of the obtained results are reported.

#### ***Molecular docking and molecular dynamic simulation***

Autodock 4.2 software package was performed for this study, briefly the crystal structure of B-RAF kinase combined with BAX was retrieved from Protein Data Bank (pdb code: 1UWH) (24). Grid and docking parameter files were generated by AutoDock Tools version 6.5.1 (25,26). For the preparation of protein, the original ligand and water molecules were removed from the coordinates and Kollman charges together with polar hydrogens were added. For ligands, Gasteiger charges were assigned and non-polar hydrogens were merged.

The grid map of  $60 \times 60 \times 60$   $\text{\AA}$  points in x, y and z directions was centered on the binding site Cys85 with a spacing of 0.375  $\text{\AA}$ . Lamarckian genetic algorithm (27) was used for docking with the following settings: a maximum number of 2500000 energy evaluations, an initial population of 300, a maximum number of 27,000 generations and 100 independent docking runs.

AutoDock Tools and visual molecular dynamics (VMD) program was used to visualize hydrophobic and hydrogen-bonding interactions between the ligand and receptor.

The best docking pose of compound **16e** with the lowest binding energy in complex with the protein structure was subjected to Gromacs 5.1.2 package (28). GROMOS96 53a6 force field (29) was used to prepare the input and topology files for the protein and the input files of the ligands were provided by means of PRODRG server (30).

Using pbc condition a box was constructed around the complex and it was solvated with simple point charge (SPC) water and 0.15 M of NaCl. A minimization step with steepest algorithm with maximum 50,000 steps was performed on the system.

Equilibration of the system was done using NVT and NPT with 1 ns in each step. Subsequently, a 30 ns MD started using time steps of 2 fs in periodic boundary condition. Leap-frog integrator together with Berendsen thermostat were used during simulation. Particle Mesh Ewald for long-range electrostatics were used using cubic interpolation.

In case of bond parameters, Lincs algorithm was used for holonomic constraints. Isotropic type of Parrinello-Rahman was used for pressure coupling in NPT ensemble. The results containing trajectories were finally subjected to VMD to analyze the binding mode of the ligand during simulation (31). Then the root mean square deviations (RMSD) and residue root mean square fluctuation (RMSF) were analyzed to study the stability and flexibility of receptor during MD. The binding dynamics was investigated by means of Hbond and distance tools during MD.

## **RESULT**

#### ***Cytotoxic and antimicrobial activities***

All the synthesized compounds were tested for cytotoxic activity against HepG2 and MCF-7 cell lines by MTT assay. The IC<sub>50</sub> value of each compound was compared with other compounds and also with the IC<sub>50</sub> value obtained for sorafenib as the lead compound. The IC<sub>50</sub> values of all compounds are given in Table 1. The results indicated that most compounds exhibited moderate to good activities against MCF-7 and HepG2 cell lines.

Compounds **15a** and **16a** without any substitution on the A ring indicated IC<sub>50</sub> values in the range of 26- 32 μM against two cell lines closed to that of sorafenib ( $P > 0.05$ ). In terms of antimicrobial and antifungal activities, only compounds **15b** and **16f** showed MIC of around 128 μg/mL and **15e** and **15f** showed MICs about 256 μg/mL against *E. coli* strain, while other compounds did not display significant antibacterial or antifungal effects.

#### Molecular docking and molecular dynamic simulation

After redocking the picture of superposition of the X-Ray crystal structures of BAX and docked structure is presented in Fig. 2 and also the binding energy calculated by AutoDock are summarized in Table 2. In order to get an insight into the diversity of poses which include location, orientation and conformation for each ligand, RMSD values of all poses were calculated based on the best pose as reference.

The RMSD table of all poses compared to the best pose for each ligand is provided but part of the main table (20 runs out of 100 runs) is presented as a sample in Table 3 due to the length of the main Table 3.

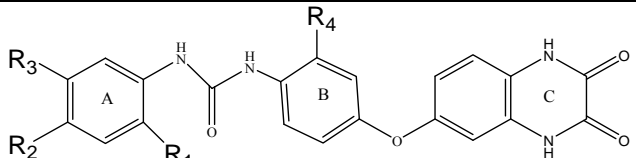
After MD simulation, the RMSD values of backbone atoms referring to the starting structure were used to monitor the dynamic stability of the MD trajectories and RMSD plot is depicted in Fig. 3a.

The MD trajectories also were analyzed to calculate of number of hydrogen bonds (H-bonds) which were formed during MD simulation (Fig. 3b).

The root mean square fluctuation (RMSF) of backbone residues was carried out to recognize the variations of protein flexibility (Fig. 3c).

The binding mode of the compound **16e** at the end of simulation is displayed in (Fig. 4). A heat map was also generated using VMD to show flexibility of the residues in the binding site during simulation as depicted in Fig. 5.

**Table 1.** The structure and IC<sub>50</sub> ± SEM values of synthesized compounds against MCF-7 and HepG2 cell lines.



Compound	R <sub>1</sub>	R <sub>2</sub>	R <sub>3</sub>	R <sub>4</sub>	IC <sub>50</sub> (μM) <sup>a</sup>	
					MCF-7	HepG2
15a	H	H	H	H	30 ± 2.51	26 ± 3.01
15b	H	H	CF <sub>3</sub>	H	10 ± 2.76***	12 ± 2.36***
15c	F	H	CF <sub>3</sub>	H	42 ± 3.55***	50 ± 2.55***
15d	Cl	H	H	H	16 ± 3.5*	10 ± 3.30***
15e	H	H	SMe	H	12 ± 2.93***	15 ± 2.07***
15f	H	Cl	CF <sub>3</sub>	H	48 ± 2.22***	45 ± 3.87***
15g	OMe	H	CF <sub>3</sub>	H	ND	ND
16a	H	H	H	Me	32 ± 3.75*	30 ± 2.25
16b	H	H	CF <sub>3</sub>	Me	10 ± 3.11***	13 ± 2.02***
16c	F	H	CF <sub>3</sub>	Me	50 ± 3.34***	50 ± 2.41***
16d	Cl	H	H	Me	18 ± 3.22*	11 ± 3.21***
16e	H	H	SMe	Me	14 ± 2.89***	17 ± 3.63*
16f	H	Cl	CF <sub>3</sub>	Me	50 ± 2.22***	48 ± 2.35***
16g	OMe	H	CF <sub>3</sub>	Me	ND	ND
Sorafenib <sup>b</sup>					25 ± 1.38	21 ± 2.14

<sup>a</sup>The values are an average of three separate determinations, <sup>b</sup>used as positive controls. SEMs were derived from the IC<sub>50</sub> values of three independent experiments. For statistical analysis one-way ANOVA was used to determine the differences between each sample and sorafenib as positive control. \* $P < 0.05$ , \*\* $P < 0.01$ , \*\*\* $P < 0.001$ ; ND, not determined.



**Fig. 2.** Comparison between the docked and the X-Ray crystal structures of BAX (yellow: docked structure; red: crystal structure).

**Table 2.** Binding energy ( $\Delta G_b$ , kcal/mol) and inhibition constants ( $K_i$ , nM) of synthesized compounds against B-RAF

Compound	$\Delta G_b$	$k_i$	Hydrophilic amino acids	Hydrophobic amino acids
15a	-11.70	2.660	Glu54, Cys85	Ile80, Phe148, Leu58, Gly146, Trp84, Phe136, Thr82
15b	-11.98	1.660	Glu54, Cys85	Gly146, Leu67, Phe148, Val 24, Trp84, Phe136, Ala34
15c	-11.85	2.070	Glu54, Cys85	Leu67, Ile66, Ile145, Leu58, Phe136, Ile16, Trp84, Phe148, Ala34, Thr82
15d	-11.82	2.150	Glu54, Cys85	Leu58, Gly146, Leu67, Phe136, Phe148, Trp84, Thr 82
15e	-12.28	1.000	Glu54, Cys85	Leu67, Leu58, Gly146, Phe136, Gln83, Lys36, Thr82
15f	-12.55	0.636	Glu54, Cys85	Ile66, Gly146, Leu58, Leu67, Trp84, Thr 82, Ala34, Phe136
15g	-11.22	5.930	Asp147	Leu67, Leu58, Gly146, Val 57, Gln83
16a	-11.96	1.710	Glu54, Cys85	Lys36, Ile80, Leu58, Gly146, Trp84, Phe136, Thr82
16b	-12.41	3.950	Glu54, Cys85	Gly146, Leu67, Leu58, Phe148, Ala34, Thr82, Phe136
16c	-11.98	1.660	Glu54	Leu67, Ile145, Ile66, Ile145, Gly146, Phe148, Gln83, Trp84, Ala34, Phe136,
16d	-11.79	2.270	Glu54	Leu58, Leu67, Gly146, Phe148, Thr82, Phe136, Trp84, Ala34, Lys36,
16e	-12.69	0.496	Asp147, Cys85	Lys 36, Leu58, His 127, Gly 146, Leu67, Phe148, Phe136, Ala34
16f	-11.89	1.930	Glu54, Cys85	Leu58, Leu67, Gly146, Phe148, Trp84, Phe136, Thr82, Gln80
16g	-11.76	2.420	Cys85	Leu67, Gly146, Val57, Leu58, Phe136, Thr82, Ala34

**Table 3.** The RMSD table of poses compared to the best pose for each ligand (run 81 to 100): RMSD values in the range 0 to 2 as blue and farther distances as red.

Run	16a	16f	16c	16e	16b	16g	16d	15a	15f	15c	15e	15b	15g	15d
81	13.39	2.48	3.47	0.00	1.85	7.37	3.19	0.36	12.70	4.53	10.80	0.63	7.54	1.60
82	1.64	12.70	10.30	3.78	12.00	15.00	2.93	11.40	3.64	4.48	3.55	1.57	3.02	13.05
83	11.36	13.20	3.56	12.30	1.36	9.73	2.51	2.78	12.70	3.27	0.87	1.47	11.70	11.40
84	11.21	1.86	12.90	10.60	1.24	0.38	1.76	0.17	12.60	0.63	13.10	1.59	2.34	0.93
85	0.90	1.88	12.50	1.43	3.52	7.22	2.99	1.09	12.9	0.65	2.47	2.30	1.56	0.16
86	1.73	12.80	3.61	11.20	12.50	11.90	10.8	0.46	1.86	1.11	10.8	1.49	15.00	3.860
87	0.94	2.70	7.74	10.70	1.33	11.30	3.00	1.34	1.82	2.49	1.10	12.3	12.10	0.00
88	10.64	15.30	12.60	7.84	10.8	12.6	11.0	1.31	2.07	12.00	0.56	1.47	2.83	0.94
89	0.967	14.80	3.39	2.01	2.21	7.31	1.30	0.96	3.27	5.18	2.00	1.09	3.40	0.617
90	12.77	11.80	12.40	1.69	0.60	1.89	10.7	0.87	1.08	2.16	0.68	0.61	11.30	11.05
91	1.43	14.80	3.52	1.28	12.00	3.76	14.70	13.60	0.60	4.33	4.05	3.13	11.20	0.97
92	2.08	2.74	11.00	1.86	2.26	0.63	2.48	0.35	1.85	0.71	12.40	4.22	12.40	1.50
93	10.83	3.07	0.00	2.18	1.21	10.9	12.40	0.58	4.29	0.64	2.57	0.65	11.6	0.96
94	11.47	12.7	10.9	1.32	13.00	3.98	2.94	1.08	12.7	12.8	0.20	2.41	11.00	0.92
95	1.37	2.66	12.50	1.28	12.00	10.70	12.50	0.47	0.97	1.21	0.91	2.27	12.00	0.94
96	0.33	3.68	9.61	2.76	13.10	11.00	2.93	1.07	10.70	3.69	2.03	4.99	4.15	11.69
97	1.16	13.00	10.20	12.9	3.47	7.69	3.14	0.90	0.60	3.17	12.40	0.23	9.87	11.20
98	1.92	13.10	7.48	3.25	0.00	11.9	10.4	1.33	1.01	3.18	0.24	2.01	12.0	2.37
99	0.88	1.98	3.77	10.70	3.52	10.90	2.26	0.92	0.17	4.38	12.90	4.66	4.40	0.89
100	1.967	2.90	3.52	14.80	11.10	3.50	1.72	0.21	0.41	4.18	12.80	12.50	10.40	1.55

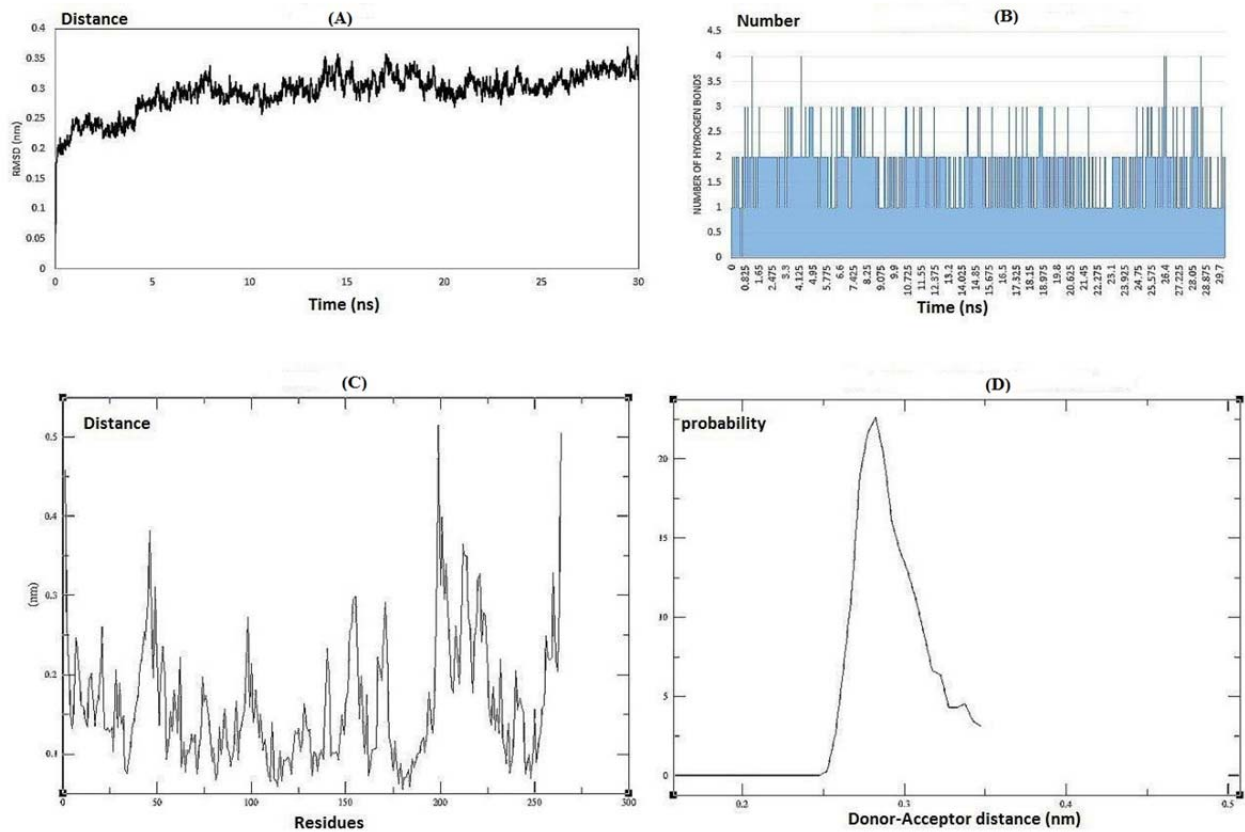


**Fig. 3.** Analysis plots of the protein backbone and ligand structure during simulation: (A) RMSD plot; (B) Plot of Hbond distribution vs time; (C) RMSF plot; (D) Plot of Hbond distribution vs distance

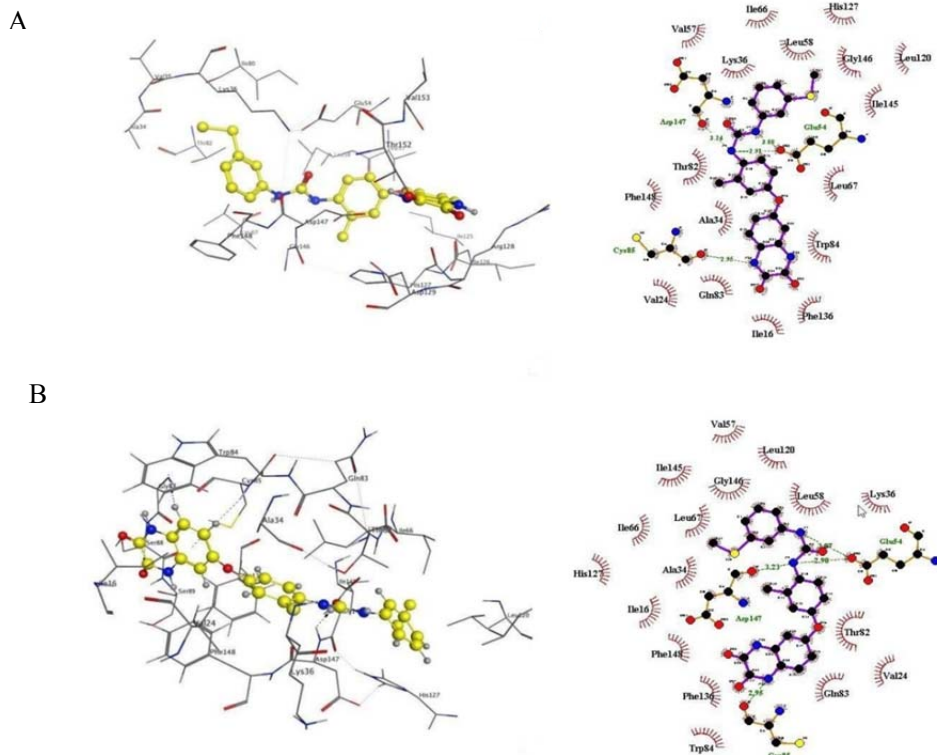


**Fig. 4.** The binding mode of 16e in the active site (A) before and (B) after simulation.



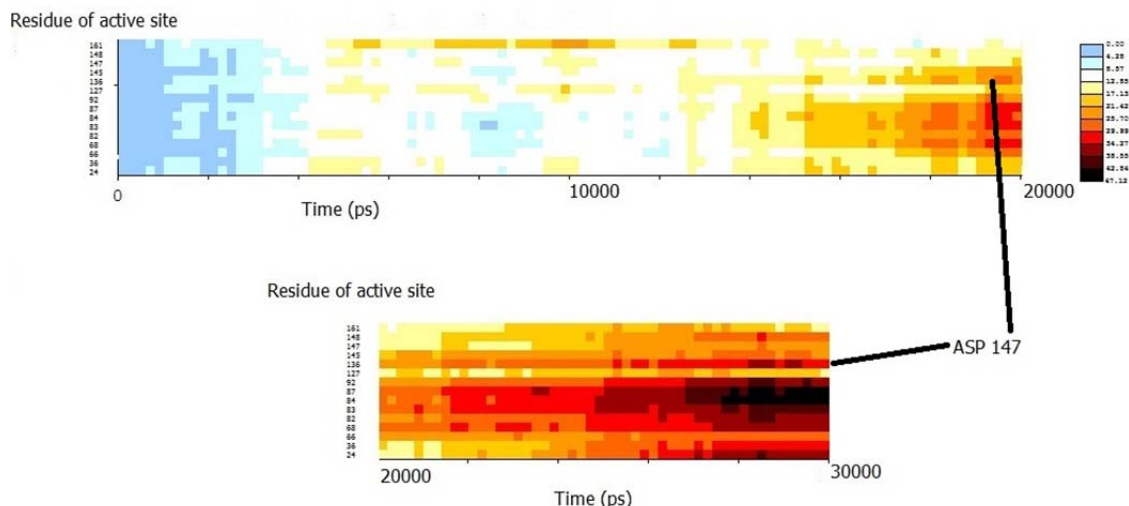


Fig. 5. Heat map of the residues in the binding site during simulation.

## DISCUSSION

The preliminary SARs showed that substitution of lipophilic groups such as  $\text{CF}_3$  or SMe at the meta position of the A ring without considering electron donating or electron withdrawing properties of substituent led to the increased activity in compounds **15b**, **16b**, **15e** and **16e** with  $\text{IC}_{50}$  values 10, 10, 12 and 14  $\mu\text{M}$  against MCF-7 cell line and 12, 13, 15 and 17  $\mu\text{M}$  against HepG2 cell line which were significantly different from  $\text{IC}_{50}$  values of parent compounds **15a** and **16a** at  $P < 0.001$ . Compounds **15d** and **16d** with a Cl substituent at the ortho position of the A ring revealed higher activity than the parent compounds (**15a**, **16a**) on the two cell lines with  $\text{IC}_{50}$  values of 16  $\mu\text{M}$  and 18  $\mu\text{M}$  on MCF-7 cells and 10 and 11  $\mu\text{M}$  on HepG2 cell line ( $P < 0.001$ ). Introduction of F group at the ortho position along with  $\text{CF}_3$  at the meta position diminished activities of compound **15c** in comparison with the compound without F group (**15b**) ( $P < 0.001$ ). Compounds **15g** and **16g** with OMe group at the ortho position along with  $\text{CF}_3$  group at the meta position showed remarkably decreased activities ( $\text{IC}_{50} > 50 \mu\text{M}$ ) compared to compounds without OMe substituent (**15b**, **16b**) in both cell lines. These results indicated that compounds with two substituents on the A ring showed less activity than compounds with one substituent (compound **15b** which have

only  $\text{CF}_3$  substituent on the A ring showed significantly different  $\text{IC}_{50}$  value compared to compounds **15c**, **15f**). On the other hand, ortho position of the A ring indicates the susceptibility to the size of the substituent, since the bulky substituent such as the OMe group, reduces significantly the activity of compounds of **15g** and **16g** compared to the small F substituent in compounds **15c** and **16c**.

Compounds **15d** and **16d** with a Cl substituent at the ortho position of the A ring revealed increased activities compared to the parent (**15a**, **16a**) compound on the two cell lines. Although antimicrobial activity has been reported for some quinoxalinedione and diaryl urea derivatives, none of these novel compounds displayed significant antibacterial or antifungal activities (32-35) which could be due to the inaccessibility of the pharmacophoric part to corresponding target sites in bacteria.

To ensure the validity of docking, the cognate ligand (BAX) was re-docked into the binding site of B-Raf kinase (PDB cod: 1UWH). The RMSD values for superposition of the cognate ligand and the best docking pose from the self-docking study was 1.6 Å (Fig. 2). This shows the validity of docking simulation for other ligands in this study. Docking results showed that these novel diaryl urea compounds were adopted properly by the B-RAF kinase binding site, suggesting that they could be potential inhibitors of B-RAF kinase.



In order to get an insight into the diversity of poses which include location, orientation and conformation for each ligand, RMSD values of all poses were calculated based on the best pose as the reference. As shown in Table 3, comparison of the RMSD of all poses to the best pose, for each ligand, the cells with RMSD values in the range 0 to 2 were highlighted as blue and the cells with farther distances were highlighted as red.

Based on this clustering approach, most poses of the ligand **15a** were in the cluster of the best pose while in case of ligand **16c** the largest RMSD distances were observed. As it can be seen, the system reached a plateau after 20 ns from the beginning of the simulation (36). RMSD plot of the protein backbone and the ligand after 30 ns of simulation is depicted in Fig. 2a. By studying the RMSD plot of the protein backbone and the ligand after 30 ns of MD simulation (Fig. 3a), it can be seen that the system reached a plateau after 20 ns from the beginning of the simulation (36) and the ligand was stable after this time and also fit in the active site and stabilized. Result of Hbond in MD showed that in most frames two hydrogen bonds were found between ligand and protein structure (Fig. 3b). It was also found that the most interactions were localized in 0.29 nm distance (Fig. 3d). As shown in Fig. 3c, RMSF plot revealed that most fluctuations of the residues were observed in C-terminal and N-terminal residues. In addition, residues ILE200, LEU150, ASP147 and ALA151 revealed considerable fluctuations during simulation. The binding mode of the compound **16e** at the end of simulation is displayed in Fig. 4. Comparing the binding mode of the compound before and after simulation shows that conformational change of the main chain in ASP147 led to the formation of a hydrogen bond between amine group in this residue and urea moiety in the ligand (Fig. 4). This result is in accord with the high flexibility of this residue during MD simulation as depicted in Fig. 5.

## CONCLUSION

In summary, a novel series of dual diaryl urea bearing quinoxalindione moiety

derivatives were screened for their cytotoxicity against two cancer cell lines. In this series of compounds we observed that replacement of pyridyl carboxamide moiety of sorafenib with rigid quinoxalindione moiety resulted compounds **15b**, **16b**, **15e**, **16e**, **15d** and **16d** which showed high potency against one or two cell lines. In addition, no significant antibacterial or antifungal activities were detected. The binding modes of all compounds at the active site of B-RAF protein were recognized by molecular docking. All compounds were perfectly placed in the active site. MD simulation analyses on compound **16e** such as RMSD, RMSF revealed that this compound is stable in B-RAF active site. This research highlights the cytotoxic potential for further development of these novel diaryl urea derivatives.

## ACKNOWLEDGMENTS

The content of this paper is extracted from the Ph.D thesis (No. 394159) submitted by Sedighe Sadeghian-Rizi which was financially supported by the Isfahan University of Medical Sciences, Isfahan, Iran.

## REFERENCES

1. Jemal A, Bray F, Center MM, Ferlay J, Ward E, Forman D. Global cancer statistics. *CA Cancer J Clin.* 2011;61(2):69-90.
2. Kim S-K. Handbook of anticancer drugs from marine origin. Springer International Publishing Switzerland. 2015: pp. 1-15.
3. Solomon VR, Hu C, Lee H. Hybrid pharmacophore design and synthesis of isatin-benzothiazole analogs for their anti-breast cancer activity. *Bioorg Med Chem.* 2009;17(21):7585-7592.
4. Noolvi MN, Patel HM, Bhardwaj V, Chauhan A. Synthesis and *in vitro* antitumor activity of substituted quinazoline and quinoxaline derivatives: search for anticancer agent. *Eur J Med Chem.* 2011;46(6):2327-2346.
5. Kim HJ, Cho HJ, Kim H, El-Gamal MI, Oh CH, Lee SH, *et al.* New diarylureas and diarylamides possessing acet(benz)amidophenyl scaffold: design, synthesis, and antiproliferative activity against melanoma cell line. *Bioorg Med Chem Lett.* 2012;22(9):3269-3273.
6. Zambon A, Ménard D, Suijkerbuijk BMJM, Niculescu-Duvaz I, Whittaker S, Niculescu-Duvaz D, *et al.* Novel hinge binder improves activity and pharmacokinetic properties of BRAF inhibitors. *J Med Chem.* 2010;53(15):5639-5655.

7. Zhao CR, Wang RQ, Li G, Xue XX, Sun CJ, Qu XJ, *et al.* Synthesis of indazole based diarylurea derivatives and their antiproliferative activity against tumor cell lines. *Bioorg Med Chem Lett.* 2013;23(7):1989-1992.
8. Sirohi B, Philip DS, Shrikhande SV. Regorafenib in gastrointestinal stromal tumors. *Future Oncol.* 2014;10(9):1581-1587.
9. Kim ST, Kim TW, Kim Kp, Kim TY, Han SW, Lee JY, *et al.* Regorafenib as salvage treatment in Korean patients with refractory metastatic colorectal cancer. *Cancer Res Treat.* 2015;47(4):790-795.
10. Wong HH, Eisen T. Tivozanib for the treatment of metastatic renal cancer. *Expert Rev Anticancer Ther.* 2013;13(6):649-660.
11. Pal SK, Bergerot PG, Figlin RA. Tivozanib: current status and future directions in the treatment of solid tumors. *Expert Opin Investig Drugs.* 2012;21(12):1851-1859.
12. Marlow M, Al-Ameedee M, Smith T, Wheeler S, Stocks MJ. Linifanib—a multi-targeted receptor tyrosine kinase inhibitor and a low molecular weight gelator. *Chem Commun.* 2015;51(29):6384-6387.
13. Toh HC, Chen PJ, Carr BI, Knox JJ, Gill S, Ansell P, *et al.* Phase 2 trial of linifanib (ABT-869) in patients with unresectable or metastatic hepatocellular carcinoma. *Cancer.* 2013;119(2):380-387.
14. Noorulla S, Sreenivasulu N, Khan A, Sayeed A. Antibacterial activity of novel substituted quinoxaline heterocycles. *Pharmanest.* 2011;2(2-3):229-238.
15. Gupta G, Verma P. Antimicrobial activity of quinoxaline derivatives. *Chem Inform.* 2015;46(4):876-884.
16. Batra S, Tusi Z, Madapa S. Medicinal chemistry of ureido derivatives as anti-infectives. *antiinfect agents. Med Chem.* 2006;5(2):135-160.
17. Doğruer DS, Uurlu Ş, Önkol T, Özçelik B, Şahin MF. Synthesis of some pyridazine derivatives carrying urea, thiourea, and sulfonamide moieties and their antimicrobial activity. *Turk J Chem.* 2010;34(1):57-65.
18. Madapa S, Tusi Z, Sridhar D, Kumar A, Siddiqi MI, Srivastava K, *et al.* Search for new pharmacophores for antimalarial activity. Part I: synthesis and antimalarial activity of new 2-methyl-6-ureido-4-quinolinamides. *Bioorg Med Chem.* 2009;17(1):203-221.
19. Sadeghian-Rizi S, Khodarahmi G, Amirhossein Sakhteman A, Jahanian-Najafabadi A, Rostami M, Mirzaei M, *et al.* Synthesis and characterization of some novel diaryl urea derivatives bearing quinoxalindione moiety. *Res Pharm Sci.* Ahead print.
20. Mosmann T. Rapid colorimetric assay for cellular growth and survival: application to proliferation and cytotoxicity assays. *J Immunol Methods.* 1983;65(1-2):55-63.
21. Freshney R. Ian . Culture of animal cells: a manual of basic technique. John Wiley and Sons, Inc. Hoboken, New Jersey. Published simultaneously in Canada. 1994: pp. 205-216.
22. Schwalbe R, Steele-Moore L, Goodwin A.C. Antimicrobial susceptibility testing protocols. New York CRC. 2007: pp. 75-79.
23. To WK, Fothergill AW, Rinaldi MG. Comparative evaluation of macrodilution and alamar colorimetric microdilution broth methods for antifungal susceptibility testing of yeast isolates. *J Clin Microbiol.* 1995;33(10):2660-2664.
24. Wan PT, Garnett MJ, Roe SM, Lee S, Niculescu-Duvaz D, Good VM, *et al.* Mechanism of activation of the RAF-ERK signaling pathway by oncogenic mutations of B-RAF. *Cell.* 2004;116(6):855-867.
25. Sanner MF. Python: a programming language for software integration and development. *J Mol Graph Model.* 1999;17(1):57-61.
26. Sadeghian-Rizi S, Sakhteman A, Hassanzadeh F. A quantitative structure-activity relationship (QSAR) study of some diaryl urea derivatives of B-RAF inhibitors. *Res Pharm Sci.* 2016;11(6):445-453.
27. Levinson NM, Kuchment O, Shen K, Young MA, Koldobskiy M, *et al.* A Src-like inactive conformation in the abl tyrosine kinase domain. *PLoS Biol.* 2006;4(5):e144.
28. Abraham MJ, Murtola T, Schulz R, Páll S, Smith JC, Hess B, *et al.* GROMACS: High performance molecular simulations through multi-level parallelism from laptops to supercomputers. *SoftwareX.* 2015;1:19-25.
29. Oostenbrink C, Villa A, Mark AE, Van Gunsteren WF. A biomolecular force field based on the free enthalpy of hydration and solvation: the GROMOS force-field parameter sets 53A5 and 53A6. *J. Comput. Chem.* 2004;25(13):1656-1676.
30. Schüttelkopf AW, Van Aalten DM. PRODRG: a tool for high-throughput crystallography of protein-ligand complexes. *Acta Crystallogr D Biol Crystallogr.* 2004;60(8):1355-1363.
31. Humphrey W, Dalke A, Schulten K. VMD: visual molecular dynamics. *J Mol Graph Model.* 1996;14(1):33-38.
32. Corona P, Carta A, Loriga M, Vitale G, Paglietti G. Synthesis and *in vitro* antitumor activity of new quinoxaline derivatives. *Eur J Med Chem.* 2009;44(4):1579-1591.
33. Grande F, Aiello F, Grazia OD, Brizzi A, Garofalo A, Neamati N. Synthesis and antitumor activities of a series of novel quinoxalinhydrazides. *Bioorg Med Chem.* 2007;15(1):288-294.
34. Tanimori S, Nishimura T, Kirihata M. Synthesis of novel quinoxaline derivatives and its cytotoxic activities. *Bioorg Med Chem Lett.* 2009;19(15):4119-4121.
35. Zarranz B, Jaso A, Aldana I, Monge A. Synthesis and anticancer activity evaluation of new 2-alkylcarbonyl and 2-benzoyl-3-trifluoromethyl-quinoxaline 1,4-di-N-oxide derivatives. *Bioorg Med Chem.* 2004;12(13):3711-3721.
36. Kumari R, Kumar R, Lynn A. g\_mmpbsa—A GROMACS tool for high-throughput MM-PBSA calculations. *J Chem Inf Model.* 2014;54(7):1951-1962.